

Hidden and detectable squeezing from microresonators

Élie Gouzien ^{1,2} Laurent Labonté,² Jean Etesse,² Alessandro Zavatta ^{3,4} Sébastien Tanzilli,² Virginia D'Auria,^{2,5,*} and Giuseppe Patera ^{6,†}

¹Université Paris–Saclay, CNRS, CEA, Institut de Physique Théorique, 91191 Gif-sur-Yvette, France

²Université Côte d'Azur, CNRS, Institut de Physique de Nice, Parc Valrose, 06108 Nice Cedex 2, France

³Istituto Nazionale di Ottica (INO-CNR) Largo Enrico Fermi 6, 50125 Firenze, Italy

⁴LENS and Department of Physics, Università di Firenze, 50019 Sesto Fiorentino, Firenze, Italy

⁵Institut Universitaire de France (IUF), France

⁶Université de Lille, CNRS, UMR 8523, Physique des Lasers Atomes et Molécules, F-59000 Lille, France



(Received 20 July 2022; accepted 5 May 2023; published 20 June 2023)

In the context of quantum integrated photonics, this work investigates the quantum properties of multimode light generated by silicon and silicon nitride microresonators pumped in pulsed regime. The developed theoretical model provides a comprehensive description of the generated quantum states. Remarkably, it shows that a full measurement of states carrying optimal squeezing levels is not accessible to standard homodyne detection, thus leaving hidden part of generated quantum features. By unveiling and discussing this behavior and possible strategies to amend it, this work proves itself essential to future quantum applications exploiting microresonators as sources of multimode states.

DOI: [10.1103/PhysRevResearch.5.023178](https://doi.org/10.1103/PhysRevResearch.5.023178)

I. INTRODUCTION

Silicon (Si) and silicon nitride (SiN) quantum photonics combine high-density integration of high-performance functions over small footprint chips [1]. In recent years, a particular interest has been driven by the possibility of exploiting their optical nonlinearities to generate on-chip multimode entanglement among frequency-time modes. Four-wave mixing (FWM) in silicon-based microresonators have been used to prove chip-scale sources of paired photons [2–4] and low-dimension quantum frequency combs [5]. More recently, experiments have started including a continuous variable (CV) regime with the demonstrations of two-color intensity [6] and quadrature [7–9] entanglement. A Si-based platform has also been validated to execute quantum algorithms that can exploit up to eight squeezed vacuum sources integrated on chip [10].

Realizations and most of theoretical models reported so far refer to Si and SiN resonators pumped in a continuous-wave regime [11,12]. At the same time, important applications in quantum metrology [13], quantum communication [14], and measurement-based quantum computing [15] can necessitate the ability to work with particularly complex entanglement structures. In this perspective, this theoretical paper addresses

the study of multipartite states produced by microresonators pumped by optical pulses. Compared to continuous wave (CW), pulsed regime offers the possibility of generating highly multimode entangled states with a much richer structure [13] as well as the possibility of tailoring entanglement features [16,17]. The presented characterization of the non-classical properties of microresonators is performed in terms of morphing supermodes, mapping the full dynamics of multipartite states into independent single-mode squeezed states whose spectral shape depends on a continuous parameter [18]. Such an analysis reveals that in standard working conditions, a full characterization of CV quantum properties of microresonators is not accessible to traditional homodyne detection, thus leaving optimal squeezing features hidden. This aspect, never considered by former works on silicon-based microresonators, is associated to quantum states whose noise spectra are asymmetrical with respect to the carrier [19,20]. Neglecting this behavior would lead to retrieving only partial information from the CV multimode source and represents a major limitation for future applications involving multimode integrated devices. In a world where integrated photonics on semiconductors is at the forefront of light-based quantum technologies, recognizing the presence of morphing behavior and hidden squeezing anticipates relevant difficulties arising from the use of microresonators as sources of multipartite quantum light. The results of this study open the door to discussions about strategies for exploiting multimode states in an optimal manner and can inspire innovative engineering techniques that facilitate the production of states that are easier to detect and manipulate in experiments. Its impact is, thus, essential for the conception and future experimental realizations of quantum technologies applications exploiting pulsed multimode states.

*virginia.dauria@univ-cotedazur.fr

†giuseppe.patera@univ-lille.fr

Published by the American Physical Society under the terms of the [Creative Commons Attribution 4.0 International](https://creativecommons.org/licenses/by/4.0/) license. Further distribution of this work must maintain attribution to the author(s) and the published article's title, journal citation, and DOI.

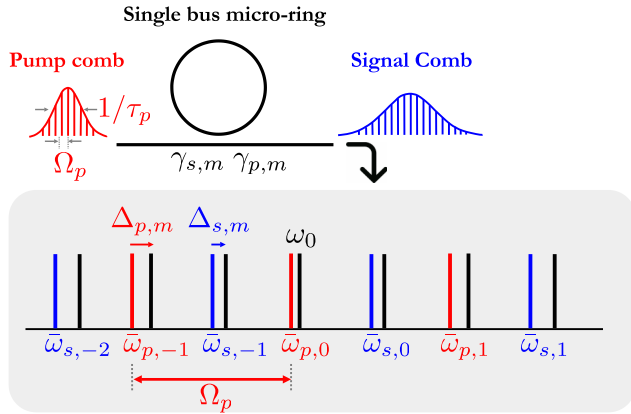


FIG. 1. Schematic of a synchronously pumped microring. The pump frequency comb has carrier $\omega_p = \bar{\omega}_{p,0}$, pulse duration τ_p , and repetition rate Ω_p approximately equal to the double of the cavity free spectral range so that the pump spectral components match one cavity resonance of two, with mode-dependent detuning $\Delta_{p,m}$. Coupling losses are given by $\gamma_{f,m}$, with $f = \{p, s\}$.

II. SYNCHRONOUSLY PUMPED MICRORINGS

As shown in Fig. 1, without losing generality, the system here investigated is a microresonator coupled to a single straight injection waveguide (single-bus device) and pumped by an infinite train of optical pulses of duration τ_p and repetition rate Ω_p . In the frequency domain, this corresponds to a comb of equally spaced spectral components,

$$\bar{\omega}_{p,m} = \omega_p + m\Omega_p \quad (1)$$

($m \in \mathbb{Z}$), spanning over a range $\sigma_p \propto 2\pi/\tau_p$ around the optical carrier at frequency ω_p . To address common experimental situations, a type-0 FWM process is considered. This phase-matching choice guarantees high nonlinear conversion efficiencies and is thus particularly compatible with the CV regime [7–9]. In the frequency domain, FWM interaction modes are determined by frequencies corresponding to the cavity resonances [21]:

$$\omega_m = \omega_0 + \sum_{k \geq 1} \frac{\Omega_k}{k!} m^k. \quad (2)$$

The reference label $m = 0$ indicates the resonance whose frequency approximately matches the pump carrier, $\omega_0 \approx \omega_p$ (see Fig. 1). The first-order parameter $\Omega_1 = c/(n_g R_{\text{eff}})$ gives the average cavity free spectral range (FSR) in terms of the speed of light in vacuum c , the group index n_g , and the ring effective radius R_{eff} . To have distinct signal and pump modes and guarantee a synchronous pumping regime, the pump repetition rate is taken to be $\Omega_p \approx 2\Omega_1$ (i.e., $\bar{\omega}_{p,m} \approx \omega_p + 2m\Omega_1$) so that the pump injection components approximately match one cavity resonance out of two. Synchronous pumping operation has been validated, in bulk quantum optics, as a particularly efficient one for the generation of high-quality CV multipartite entanglement for quantum computing and quantum metrology applications [22].

Due to dispersion, their detuning with respect to even cavity resonances $\Delta_{p,m} = \omega_{2m} - \bar{\omega}_{p,m}$ changes with m . The parameter $\Omega_2 = -(n'_g c^2)/(n_g^3 R_{\text{eff}}^2)$ accounts for second-order

dispersion effects via the frequency derivative n'_g together with higher-order dispersion terms $\Omega_{k>2}$. As depicted in Fig. 1, frequency-entangled signal modes are generated by FWM at frequencies

$$\bar{\omega}_{s,m} = \omega_p + (2m + 1) \frac{\Omega_p}{2} \quad (3)$$

and can thus be unequivocally distinguished from the pump (“s” denotes “signal”). They are in general detuned by $\Delta_{s,m} = \omega_{2m+1} - \bar{\omega}_{s,m}$ with respect to the odd cavity resonances.

III. SYSTEM HAMILTONIAN

The quantum evolution of the microring is obtained in terms of the bosonic operators associated to the pump (\hat{p}_m) and signal (\hat{s}_m) intracavity modes verifying the standard boson commutation rules and the only nonzero commutators are

$$\begin{aligned} [\hat{p}_m, \hat{p}_n^\dagger] &= \delta_{m,n}, \\ [\hat{s}_m, \hat{s}_n^\dagger] &= \delta_{m,n}. \end{aligned} \quad (4)$$

In order to correctly keep into account dispersion, field quantification is performed by choosing the displacement field $\hat{\mathbf{D}}$ and the magnetic field $\hat{\mathbf{B}}$ as the fundamental entities [23–25] (more details are given in Appendix A). The dynamics of the intracavity modes is ruled by the system total Hamiltonian,

$$H_{\text{tot}} = H_0 + H_{\text{int}} + H_{\text{inj}}, \quad (5)$$

where

$$\hat{H}_0 = \sum_m \hbar \omega_{p,m} \hat{p}_m^\dagger \hat{p}_m + \sum_m \hbar \omega_{s,m} \hat{s}_m^\dagger \hat{s}_m \quad (6)$$

is the Hamiltonian of the free fields and

$$\hat{H}_{\text{inj}} = i\hbar \sum_m (\mathcal{E}_m \hat{p}_m^\dagger e^{-i\bar{\omega}_{p,m}t} + \mathcal{E}_m^* \hat{p}_m e^{i\bar{\omega}_{p,m}t}) \quad (7)$$

describes the injection of a frequency comb (synchronous pumping) with spectral amplitudes \mathcal{E}_m at frequencies $\bar{\omega}_{p,m}$. In the context of a scalar theory (see Appendix A), the interaction Hamiltonian, \hat{H}_{int} , can be written in terms of the displacement field inside the microresonator as:

$$\hat{H}_{\text{int}} = \frac{\eta^{(3)}}{4} \int \hat{D}^4 d^3 \mathbf{r}, \quad (8)$$

with $\eta^{(3)}$ the inverse permittivity tensor and by assuming a medium with null second-order susceptibility. In the rotating-wave approximation, only three kinds of processes (and their reciprocal) respect the energy conservation condition and must be kept in the explicit expression of the Hamiltonian of (8). The first process describes the conversion of two pump photons into two other pump photons such that $\omega_{p,m} + \omega_{p,n} = \omega_{p,l} + \omega_{p,k}$; the second of two pump photons into two signal photons such that $\omega_{p,m} + \omega_{p,n} = \omega_{s,l} + \omega_{s,k}$; the third of one pump photon and one signal photon to another couple of pump and signal photons such that $\omega_{p,m} + \omega_{s,n} = \omega_{p,l} + \omega_{s,k}$. The processes $\omega_{s,m} + \omega_{s,n} = \omega_{s,l} + \omega_{s,k}$ will be neglected because, in the semiclassical approximation, they are mediated by amplitudes that have null mean value ($\langle \hat{s}_m \rangle = 0$). Accordingly, the interaction Hamiltonian can be written as:

$$\hat{H}_{\text{int}} \approx \hat{H}_{p,p} + \hat{H}_{p,s}, \quad (9)$$

where the term $\hat{H}_{p,p}$ describes the FWM interaction between pump modes and the term $\hat{H}_{p,s}$ describes the pump-mediated generation of the signal modes. The details of these two terms are given in Appendix B [Eqs. (B1) and (B2)].

IV. MULTIMODE QUANTUM LANGEVIN EQUATIONS

Quantum properties of multimode light out of the microresonator are obtained by solving the system of coupled quantum Langevin equations describing its dissipative dynamics [26,27]. These are obtained through standard methods [28] from the system Hamiltonian (5) and after moving in the rotating frame of the injection as detailed in Appendix C. They can be cast as follows:

$$\frac{d}{dt}\hat{\xi} = \mathcal{L}\hat{\xi} + N(\hat{\xi}) + \mathcal{F}\hat{\xi}_{\text{in}} + \mathcal{E} \quad (10)$$

with the column vectors $\hat{\xi} = (\hat{p}|\hat{s})^T$, $\hat{p} = (\dots, \hat{p}_{-1}, \hat{p}_0, \hat{p}_1 \dots)^T$ and $\hat{s} = (\dots, \hat{s}_{-1}, \hat{s}_0, \hat{s}_1 \dots)^T$ collecting the pump and signal intracavity field operators, $\hat{\xi}_{\text{in}} = (\hat{p}_{\text{in}}|\hat{q}_{\text{in}}|\hat{s}_{\text{in}}|\hat{r}_{\text{in}})^T$ the additive noise terms and \mathcal{E} the external driving of the pump modes. In particular \hat{p}_{in} and \hat{s}_{in} account for pump and signal coupling losses, while \hat{q}_{in} and \hat{r}_{in} for pump and signal propagation losses. In Eq. (10), the nonlinear evolution of intracavity modes is described by $N(\hat{\xi})$. Its explicit expression as a function of the elements of $\hat{\xi}$ is provided by Eqs. (C7) and (C8). The diagonal matrix \mathcal{L} accounts for the linear part of the evolution and is given by

$$\mathcal{L} = \left(\begin{array}{c|c} \mathcal{L}_p & 0 \\ \hline 0 & \mathcal{L}_s \end{array} \right), \quad (11)$$

where \mathcal{L}_f (with $f \in \{p, s\}$) are diagonal matrices with elements

$$\mathcal{L}_{f,j} = -\gamma_{f,j} - \kappa_{f,j} - i\Delta_{f,j}, \quad (12)$$

which contain mode-dependent coupling losses $\gamma_{f,j}$ and detunings $\Delta_{f,j}$. The terms $\kappa_{f,j}$ account instead for intracavity losses. The noise matrix \mathcal{F} is

$$\mathcal{F} = \left(\begin{array}{c|c|c|c} \mathcal{F}_p & \mathcal{F}_q & 0 & 0 \\ \hline 0 & 0 & \mathcal{F}_s & \mathcal{F}_r \end{array} \right), \quad (13)$$

where each block is diagonal with elements $\mathcal{F}_{p,j} = \sqrt{2\gamma_{p,j}}$, $\mathcal{F}_{q,j} = \sqrt{2\kappa_{p,j}}$, $\mathcal{F}_{s,j} = \sqrt{2\gamma_{s,j}}$, and $\mathcal{F}_{r,j} = \sqrt{2\kappa_{s,j}}$.

Linearized quantum Langevin equations

Langevin equations are linearized around a stable classical stationary solution of the nonlinear system of algebraic equations that one obtains from Eq. (10). The linearization is made by approximating the field operators $\hat{\xi}$ by $\langle \hat{\xi} \rangle + \delta\hat{\xi}$, where $\delta\hat{\xi}$ is a perturbation assumed small with respect to $\langle \hat{\xi} \rangle$, and neglecting in Eq. (10) terms of higher order than the first in $\delta\hat{\xi}$. The equations for finding the classical stationary solution (i.e., for the $\langle \hat{\xi} \rangle$) read as:

$$\mathcal{L}\langle \hat{\xi} \rangle + \langle N(\hat{\xi}) \rangle + \mathcal{E} = 0, \quad (14)$$

where the pump modes are macroscopically populated, $\langle \hat{p}_m \rangle \neq 0$, and the signal modes are empty, $\langle \hat{s}_m \rangle = 0$. This corresponds to a below threshold regime. The solutions $\langle \hat{p}_m \rangle$

depend on the injected pump power P , the detuning $\Delta_{p,0}$, and the FSR mismatch $\Delta\Omega = \Omega_1 - \Omega_p/2$. The linear quantum Langevin equations that are obtained from this procedure corresponds to a double-bus model since they include both coupling and internal losses (see Appendix D). However, they can be conveniently expressed in terms of a single-bus model after a suitable redefinition of the noise terms as detailed in Appendix E.

In what follows, the linearized Langevin equations for fluctuation operators $\delta\hat{\xi}$ will be expressed in terms of the quadrature operators associated to intracavity modes: quadratures are indeed observables that, in principle, can be measured in experiments. By defining $\hat{x}_m = (1/\sqrt{2})(\hat{s}_m^\dagger + \hat{s}_m)$ $\hat{y}_m = (i/\sqrt{2})(\hat{s}_m^\dagger - \hat{s}_m)$, one obtains the following set of coupled quantum linear Langevin equations:

$$\frac{d\hat{\mathbf{R}}(t)}{dt} = (-\Gamma + \mathcal{M})\hat{\mathbf{R}}(t) + \sqrt{2\Gamma}\hat{\mathbf{R}}_{\text{in}}(t), \quad (15)$$

where $\hat{\mathbf{R}}(t) = (\hat{\mathbf{x}}(t)|\hat{\mathbf{y}}(t))^T$ is the column vector $\hat{\mathbf{x}}(t) = (\dots, \hat{x}_{-1}, \hat{x}_0, \hat{x}_{+1}, \dots)^T$ and $\hat{\mathbf{y}}(t) = (\dots, \hat{y}_{-1}, \hat{y}_0, \hat{y}_{+1}, \dots)^T$ while $\hat{\mathbf{R}}_{\text{in}}(t)$ contains the quadratures of the input signal modes, here set in the vacuum state. The diagonal matrix Γ describes mode-dependent coupling losses of the single-bus cavity including propagation losses as well (see Appendix E and Ref. [29]). The interaction matrix \mathcal{M} is expressed as

$$\mathcal{M} = \left(\begin{array}{c|c} \text{Im}[G + F] & \text{Re}[G - F] \\ \hline -\text{Re}[G + F] & -\text{Im}[G + F]^T \end{array} \right), \quad (16)$$

in terms of the complex matrices G and F (with $G = G^\dagger$ and $F = F^T$ [30]). Matrix G contains mode-dependent detunings and all terms accounting for self- and cross-phase modulation (referred here as nonlinear dispersion terms), while F accounts for parametric amplification processes. For the microresonator model considered here, their elements explicitly depend on the pump stable steady states as:

$$F_{m,n} = g \sum_l \langle \hat{p}_{m-l+n+1} \rangle \langle \hat{p}_l \rangle, \quad (17)$$

$$G_{m,n} = \Delta_{s,m} \delta_{[m-n]} + g \sum_l 2 \langle \hat{p}_{m+l-n} \rangle \langle \hat{p}_l \rangle^*, \quad (18)$$

where $\delta_{[m-n]}$ is the Kronecker delta and g the nonlinear strength. The output quadratures $\hat{\mathbf{R}}_{\text{out}}$ can be obtained via input-output relations $\hat{\mathbf{R}}_{\text{in}} + \hat{\mathbf{R}}_{\text{out}} = \sqrt{2\Gamma}\hat{\mathbf{R}}$ [28]. In the Fourier space, input and output quadratures are connected via the transfer function, $S(\omega)$, that solves Eq. (15) as

$$\hat{\mathbf{R}}_{\text{out}}(\omega) = S(\omega)\hat{\mathbf{R}}_{\text{in}}(\omega), \quad (19)$$

where $\omega \in \mathbb{R}$. The complex matrix-valued function $S(\omega)$ is found to be

$$S(\omega) = \sqrt{2\Gamma}(i\omega I + \Gamma - \mathcal{M})^{-1}\sqrt{2\Gamma} - I. \quad (20)$$

Since \mathcal{M} is Hamiltonian and Γ is skew-Hamiltonian, it is possible to prove [18] that $S(\omega)$ is ω -symplectic [31], so that $\hat{\mathbf{R}}_{\text{out}}(\omega)$ are the Fourier transform of *bona fide* boson quadrature operators that satisfy the property $\hat{\mathbf{R}}^\dagger(\omega) = \hat{\mathbf{R}}(-\omega)$ so as to ensure the Hermiticity in time domain [32].

V. MORPHING SUPERMODES ANALYSIS

As demonstrated in Ref. [18], in the general case of a system presenting both linear and nonlinear dispersion (in G) and parametric amplification (in F), squeezing properties need to be described in terms of *morphing supermodes*. These are coherent superpositions of the original modes that evolve with a continuous parameter (here ω) and allow mapping multimode CV entangled states into a collection of independent squeezed states. They are obtained by performing the analytic Bloch-Messiah decomposition (ABMD) of the transfer function $S(\omega) = U(\omega)D(\omega)V^\dagger(\omega)$. In this expression, $U(\omega)$ and $V(\omega)$ are unitary and ω -symplectic matrix-valued functions that characterize the supermodes structure. In particular, the output quadratures of morphing supermodes are given by

$$\hat{\mathbf{R}}'_{\text{out}}(\omega) = U^\dagger(\omega)\hat{\mathbf{R}}_{\text{out}}(\omega) \quad (21)$$

and represent the optimally (anti-)squeezed operators. In particular their noise level is given by the elements of the diagonal matrix $D(\omega) = \text{diag}\{d_1(\omega), \dots, d_N(\omega)|d_1^{-1}(\omega), \dots, d_N^{-1}(\omega)\}$, where $d_i^{-1}(\omega)$ is the squeezing of supermode “ i ” and $d_i(\omega)$ the antisqueezing of supermode “ $N+i$ ” [with $d_i(\omega) \geq 1$ for all ω]. In time domain, assuming input vacuum state, the stationary Gaussian quantum state at the microresonator output is entirely characterized by the covariance matrix $\sigma_{\text{out}}(t) = \frac{1}{2}(\hat{\mathbf{R}}_{\text{out}}(0)\hat{\mathbf{R}}_{\text{out}}^T(t) + \hat{\mathbf{R}}_{\text{out}}(t)\hat{\mathbf{R}}_{\text{out}}^T(0))^T$ [33]. In Fourier domain it corresponds to the spectral covariance matrix,

$$\sigma_{\text{out}}(\omega) = \frac{1}{2\sqrt{2\pi}}U(\omega)D^2(\omega)U^\dagger(\omega), \quad (22)$$

that, in general, is Hermitian since $D(\omega)$ is real. While this analysis in terms of morphing supermodes allows to fully characterize the quantum properties of synchronously pumped microresonators, it generally applies to the dynamics induced by any quadratic Hamiltonian [18]. The generated states belong to the broad class of Gaussian states having a Hermitian covariance matrix as like (22). Discussed results can thus be easily extended to many other situations.

VI. MULTIMODE SQUEEZING FROM A MICRO-RESONATOR

As a representative example, in what follows, it will be considered the case of a pump frequency comb of spectral amplitudes $\{\mathcal{E}_m\}_{m \in \mathbb{Z}}$ with Gaussian distribution $\mathcal{E}_0 \exp[-m^2/(2\sigma_p)]$, resonant with the central cavity mode $m=0$, i.e., $\Delta_0=0$ [Fig. 2 (top)]. Its repetition rate matches the double of the cavity average FSR ($\Delta\Omega=0$), the spectral width is $\sigma_p=20$ and \mathcal{E}_0 is set so that the system is 1% below its oscillation threshold. Cavity losses are equal $\gamma_m=\gamma$ for all m and second-order anomalous dispersion is set to $\Omega_2=-0.01\gamma$. As illustrated in Fig. 2, the real Gaussian injection profile (top) induces a complex intracavity steady state (bottom) whose amplitude and phase spectra enter the systems dynamics via Eqs. (17) and (18). Correspondingly, Fig. 3 shows optimal squeezing $[d_i^{-1}(\omega)]$ and antisqueezing $[d_i(\omega)]$ levels as functions of ω , as obtained by ABMD. The highest (anti-)squeezing value is obtained at $\omega=0$ for supermode $i=1$ ($i=N+1$). Figure 4 (top)

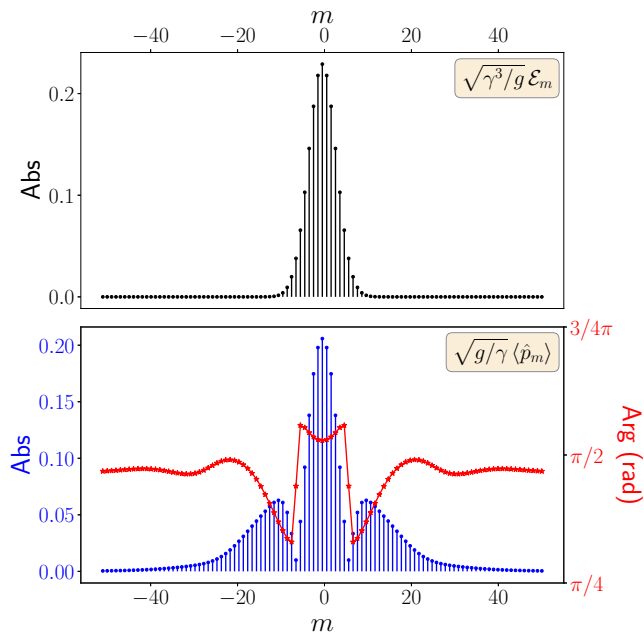


FIG. 2. (Top) Normalized amplitude and phase profiles of the injection $\sqrt{\gamma^3/g}\mathcal{E}_m$ and (bottom) of intracavity steady-state solutions $\sqrt{g/\gamma}\langle\hat{p}_m\rangle$. The stable steady state $\langle\hat{p}_m\rangle$ is obtained by solving the classical part of the nonlinear Langevin equations for a space of $N=101$ pump modes. Parameters: $\mathcal{E}_m = \mathcal{E}_0 \exp[-m^2/(2\sigma_p)]$ with $\sigma_p=20$ and \mathcal{E}_0 is chosen so that the system is 1% below its threshold; $\Delta_0/\gamma=0$, $\Delta\Omega/\gamma=0$, $\Omega_2/\gamma=-0.01$ and losses equal to γ for all m .

shows the frequency-varying coefficients of the first morphing supermode given by the first column of $U(\omega)$, say, $U_1(\omega)$. Higher-order supermodes are reproduced in Appendix F (see Fig. 7). In agreement with Eq. (21), Fig. 4 (bottom) illustrates how, at a given $\bar{\omega}$, the supermode quadrature is built as $\hat{\mathbf{R}}'_{\text{out},1}(\bar{\omega}) = (\text{Re}[U_1^T(\bar{\omega})] - i \text{Im}[U_1^T(\bar{\omega})])\hat{\mathbf{R}}_{\text{out}}(\omega)$.

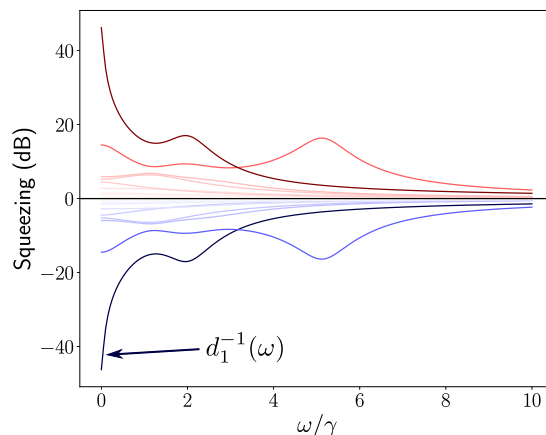


FIG. 3. Frequency-dependent optimal degree of antisqueezing $d_i(\omega)$ (shades of red) and squeezing $d_i^{-1}(\omega)$ (shades of blue), respectively. The zero level represents the standard quantum limit. The function $d_1^{-1}(\omega)$ corresponds to the optimal level of squeezing associated to the morphing supermode $U_1(\omega)$ in Fig. 4. Simulation parameters as in Fig. 2.

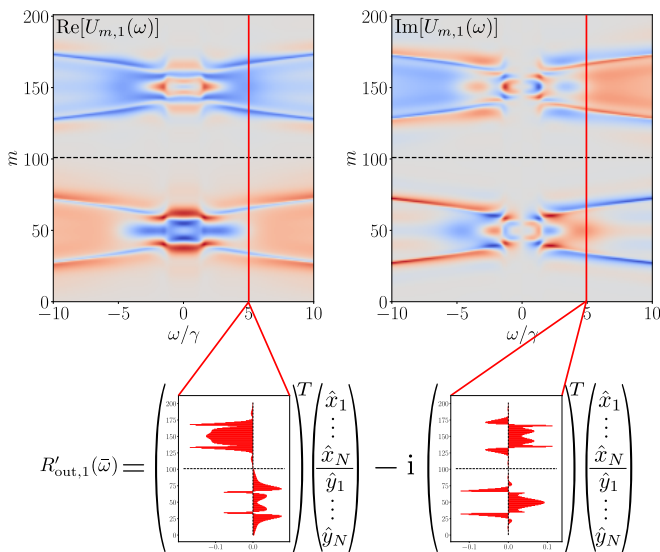


FIG. 4. Top: Real and imaginary part of the first output morphing supermode for the case of a microresonator. Bottom: For a given frequency $\bar{\omega}$, the column vectors of the real and imaginary part of $U_1(\omega)$ give the coefficients of the supermode quadrature $R'_{out,1}(\bar{\omega})$. They also define the profile a local oscillator should have to detect the optimal level of squeezing $d_1^{-1}(\bar{\omega})$ (see Fig. 3). Simulation parameters as in Fig. 2.

Changing the analysis frequency thus implies a different linear combination. As numerically shown, ABMD generally returns supermodes whose structure smoothly depends on ω and have both real and imaginary parts non-null. As a consequence, the multimode state produced by the microresonator is characterized by a $\sigma_{out}(\omega)$ that, contrarily to what was assumed in previous studies, is not real. This formally reflects the presence of an imbalance between the noise spectral components at ω and $-\omega$ [19,20]. Such an effect is characteristic of a dynamics in a $\chi^{(3)}$ medium and of a mode-dependent dispersion. It is not present in dispersion-compensated nonlinear cavities with $\chi^{(2)}$ media where $G = 0$ and, correspondingly, the supermodes are frequency independent and real in the quadrature representation [17,27].

VII. HOMODYNE DETECTION AND MEASURABLE SQUEEZING

In experiments, the spectral covariance matrix of Eq. (22) can be reconstructed via frequency homodyning [34]: a reference beam, called “local oscillator” (LO):

$$E_{LO}(t) = i \sum_m \alpha_m e^{-i\omega_s t} + \text{H.c.}, \quad (23)$$

beats with the microresonator output so that the photocurrent operator can be written as

$$\begin{aligned} \hat{i}(t) &\propto \sum_m \{\text{Re}[\alpha_m] \hat{x}_{out,m}(t) + \text{Im}[\alpha_m] \hat{y}_{out,m}(t)\} \\ &= \mathbf{Q}^T \cdot \hat{\mathbf{R}}_{out}(t). \end{aligned} \quad (24)$$

Here the normalized column vector $\mathbf{Q} = (\text{Re}[\alpha] | \text{Im}[\alpha])^T$ corresponds to the spectral profile of the LO in the quadra-

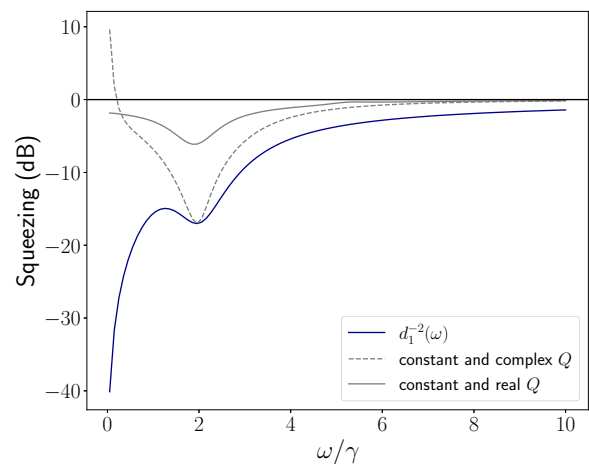


FIG. 5. Comparison between the optimal squeezing of the first supermode (solid blue) as shown in Fig. 3, the squeezing one would measure, via homodyne detection, with an unphysical ω -independent complex LO quadrature profile (dashed gray), the optimal squeezing accessible to a standard homodyne detection (solid gray). Simulation parameters as in Fig. 2.

ture representation and collects the complex LO amplitudes $\alpha = (\dots, \alpha_{-1}, \alpha_0, \alpha_{+1}, \dots)^T$. Although LOs with arbitrary spectral amplitudes α are accessible to experiments [22], the amplitudes and phases of their spectral components always combine so as to give real quadratures, i.e., a real \mathbf{Q} : This guarantees that, in time domain, the LO electric field (23) and the photocurrent operator (24) are Hermitian. Equation (24) has been obtained by assuming that the microresonator output varies little during the detection time and that the actual detection time is longer than Ω^{-1} . In experiments, this assumption is easily verified for standard microring resonators for which the output slowly varying envelope is in the tens of MHz, Ω in the hundreds of THz and detection time typically of the order of tens of ns [1]. When the Fourier transform of the photodetection signal is performed, such a projective measurement allows retrieving the field quadratures and, in particular, the measured noise spectrum:

$$\Sigma_{\mathbf{Q}}(\omega) = \mathbf{Q}^T \sigma_{out}(\omega) \mathbf{Q}. \quad (25)$$

In this context, ω is indicated as the analysis frequency as it directly identifies a given noise component of the photocurrent signal. By inserting Eq. (22) in (25), it is evident that optimal (anti-)squeezing $d_i^{-1}(\omega)$ [$d_i(\omega)$] can be measured only if \mathbf{Q} matches the i th column of $U(\omega)$ for all ω [i.e., $U(\omega)$ projects optimally on the LO]. However, in general, this is not possible for two reasons: (i) \mathbf{Q} should depend on ω and (ii) \mathbf{Q} is real while $U(\omega)$ can be complex. In the case $U(\omega)$ is real and \mathbf{Q} constant, the homodyne detection can detect optimal squeezing only at the frequency $\bar{\omega}$ for which the local oscillator matches the supermode profile [$\mathbf{Q}^T U_1(\bar{\omega}) = 1$]. Reconstructing the entire squeezing profile is done by reshaping \mathbf{Q} for each $\bar{\omega}$. On the other hand, since in general $U(\omega)$ is complex, LO cannot be mode matched to any supermode. Thus, homodyne measure is suboptimal for all values of ω and part of the quantum properties of the output state remains hidden. As a way of example, Fig. 5 compares the optimal squeezing

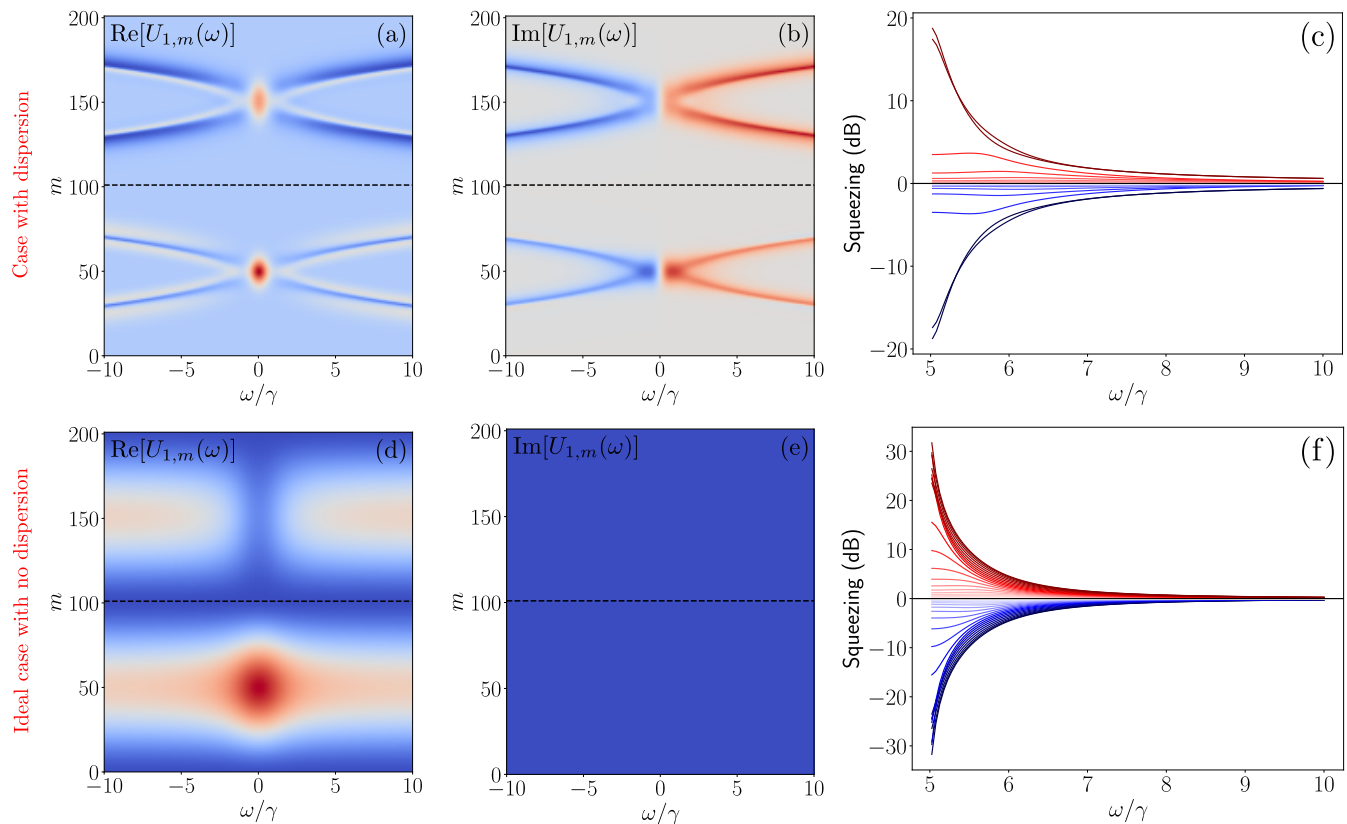


FIG. 6. Case of Gaussian intracavity steady-state solution $\langle \hat{p}_m \rangle = A \exp[-(m - \bar{m})^2/2\sigma]$: Real (a) [respectively (d)] and imaginary (b) [respectively (e)] part of the first morphing supermode and spectrum of the frequency-dependent singular values (c) [respectively (f)] $d_1^2(\omega)$ and $d_1^{-2}(\omega)$ in the case of microring with dispersion (respectively ideal case without dispersion). Parameters: $A = 0.16$, $\sigma = 10$, $\Delta_0/\gamma = -2$, $\Delta\Omega = 0$, and [(a)–(c)] $\bar{m} = 0$, $\Omega_2/\gamma = -0.01$; [(d)–(f)] $\bar{m} = 0.5$, $\Omega_2 = 0$, with losses equal to γ for all m .

spectrum $d_1^{-2}(\omega)$ (solid blue line) of the first morphing supermode $U_1(\omega)$ to the one obtained by using an ω -independent LO profile. If a LO with complex quadrature coefficients were possible, then a perfect mode match of Q to U_1 would be possible only at a given frequency $\bar{\omega}$ ($\approx 2/\gamma$ in the example): This would lead to a noise spectrum as given by the dashed gray line in the figure, making it possible to detect optimal squeezing at least at this frequency. However, as complex Q are not physically possible, in experiments, the best one could do is to optimize Q around $\bar{\omega}$ so that the detected squeezing is the closest as possible to the optimal value given by $d_1^{-2}(\bar{\omega})$. The optimal Q is obtained as the eigenvector corresponding to the extremal eigenvalue of $\text{Re}[\sigma_{\text{out}}(\bar{\omega})]$. In this case the detected noise spectrum (solid gray line) never reaches the values of optimal squeezing. In order to detect optimal squeezing at all frequencies, the LO profile should be a complex-valued smooth function of ω . This cannot be implemented in standard detection schemes and rather requires an interferometer with memory effect associating balanced detection with external analysis cavities. The description of this scheme is beyond the scope of this work and will be treated in a subsequent publication.

Note that the CW pumping regime is a special case of the pulsed regime we are considering in this work. Below threshold, the system can be reduced to a collection of independent detuned two-mode OPO where the morphing behavior is still present but the squeezing is not “hidden.” On the other side,

above threshold, modulational instability gives rise to multi-mode behavior such as the self pulsing regime. This case then falls under the situation considered in this work and presents “hidden squeezing.” Complex morphing supermodes are obtained for a vast majority of configurations. From a physical point of view, this behavior is due to a nontrivial G whose effect is to scramble the quantum correlations generated through F and induce an imbalance in the noise spectrum. Engineering strategies of the injection can be considered in order to limit these effects. Figure 6 (top) shows the first morphing supermode as obtained when the injection $\{\mathcal{E}_m\}_{m \in \mathbb{Z}}$ is engineered to obtain the intracavity steady state $\langle \hat{p}_m \rangle = A \exp[-(m - \bar{m})^2/2\sigma]$, with $A = 0.16$, $\bar{m} = 0$ and keeping all the other parameters as in the previous example. This supermode shows a simpler frequency dependence but a nontrivial imaginary part as well as a somehow reduced level of squeezing due to an increased distance from the threshold. Better results are obtained when $\bar{m} = 0.5$ and in the ideal case in which dispersion is negligible ($\Omega_2 = 0$). In this case, shown in Fig. 6 (bottom), the first few supermodes are weakly depending on ω and are real. This makes their squeezing properties completely accessible through a standard homodyne measurement. Higher-order supermodes are reproduced in Appendix F (see Figs. 8 and 9). Although chromatic dispersion can be reduced thanks to tailored waveguide geometries [35,36], in the real world, reaching optimal conditions can be hard. In this sense, the current theoretical analysis opens the route to

more sophisticated engineering approaches that could allow future devices to get closer to such ideal configurations.

VIII. CONCLUSIONS

This work provides a complete characterization of the multimode quantum properties of pulsed microring resonators. The analysis is done in terms of squeezed morphing supermodes [18] and shows that such supermodes are in general complex, with the consequence of leaving optimal squeezing hidden to standard homodyne detection. It is crucial to be aware of this phenomenon, as it can have significant implications for experiments that require high levels of multimode squeezing, particularly in the field of quantum information science [15]. In order to cope with the unavoidable presence of morphing and hidden squeezing in integrated platforms, two strategies can be pursued: The first strategy involves carefully designing experimental configurations, including the spectral profile of the pump and possibly the resonator itself so as to reduce dispersion effects, in order to obtain real supermodes with a weak dependence on ω . The second strategy involves the conception of new measurement strategies that can allow retrieving multimode nonclassical properties in an optimal way. The phenomenon unveiled in this work is not restricted to the case of microring resonators, but is more general and concerns all physical processes for which the linearized dynamics of quantum fluctuation around stable equilibrium points can be described by a quadratic Hamiltonian containing terms such as in the matrices G and F discussed in this paper. This is the case, for example, of optomechanical systems, FWM in atomic ensembles, semiconductor microcavities and quantum cascade lasers.

ACKNOWLEDGMENTS

We acknowledge fruitful discussions about analytic decompositions with Alessandro Pugliese and about spectral covariance matrix with Carlos Navarrete-Benlloch. This work has been conducted within the framework of the project SPHIFA (ANR-20-CE47-0012). V.D'A. acknowledges financial support from the Institut Universitaire de France (IUF).

APPENDIX A: FIELD QUANTIFICATION

In order to distinguish the intracavity modes that are populated by the external pump and those that are not, we decompose the displacement field $\hat{\mathbf{D}}$ (bold designates vector quantities) as

$$\hat{\mathbf{D}}(\mathbf{r}, t) = [\hat{\mathbf{D}}_p(\mathbf{r}, t) + \hat{\mathbf{D}}_s(\mathbf{r}, t)], \quad (\text{A1})$$

where

$$\hat{D}_p(\mathbf{r}, t) = i \sum_m \mathcal{D}_{p,m} [\hat{p}_m \mathbf{d}_{p,m}(\mathbf{r}) + \hat{p}_m^\dagger \mathbf{d}_{p,m}^*(\mathbf{r})], \quad (\text{A2})$$

$$\hat{D}_s(\mathbf{r}, t) = i \sum_m \mathcal{D}_{s,m} [\hat{s}_m \mathbf{d}_{s,m}(\mathbf{r}) + \hat{s}_m^\dagger \mathbf{d}_{s,m}^*(\mathbf{r})]. \quad (\text{A3})$$

The spatial modes $\mathbf{d}_{f,m}(\mathbf{r})$ (with $f \in \{p, s\}$) corresponding to the cavity resonances are found by solving the following equations:

$$\nabla \wedge \left[\frac{1}{n^2(\mathbf{r}, \omega_m)} \nabla \wedge \mathbf{b}_{f,m}(\mathbf{r}) \right] = \frac{\omega_m^2}{c^2} \mathbf{b}_{f,m}(\mathbf{r}), \quad (\text{A4})$$

$$\mathbf{d}_{f,m}(\mathbf{r}) = \frac{ic}{\omega_{f,m}} \nabla \wedge \mathbf{b}_{f,m}(\mathbf{r}). \quad (\text{A5})$$

They are normalized such as

$$\int d^3\mathbf{r} \frac{\mathbf{d}_{f,m}^*(\mathbf{r}) \cdot \mathbf{d}_{f,m}(\mathbf{r})}{\epsilon_0 n^2(\mathbf{r}, \omega_{f,m})} \frac{v_\phi(\omega_{f,m})}{v_g(\omega_{f,m})} = 1, \quad (\text{A6})$$

where $v_\phi(\omega_{f,m})$ and $v_g(\omega_{f,m})$ are the phase and group velocities, respectively. The operators $\hat{p}_m(t)$ and $\hat{s}_m(t)$ are the slowly varying annihilation field amplitudes for pump and signal fields. They destroy one elemental excitation in the pump (respectively signal) mode $\mathbf{d}_{p,m}(\mathbf{r})$ (respectively, $\mathbf{d}_{s,m}(\mathbf{r})$) and verify the standard boson commutation rules (4).

The quantities $\mathcal{D}_{f,m}$ (with $f \in \{p, s\}$) are given by

$$\mathcal{D}_{f,m} = \sqrt{\frac{\epsilon_0 \hbar \omega_{f,m}}{2}} \quad (\text{A7})$$

and can be interpreted as the single polariton field amplitudes in the mode $\mathbf{d}_{f,m}(\mathbf{r})$.

In the semivectorial approximation [21] the cavity sustains quasi-TE and quasi-TM modes such that $\mathbf{b}_m(\mathbf{r}) = T(r, z) Y_m(\theta) \mathbf{u}$ in cylindrical coordinates (r, θ, z) , with $\mathbf{u} \in \{\mathbf{u}_{\text{TE}}, \mathbf{u}_{\text{TM}}\}$ the mode polarization, $T(r, z)$ and $Y_m(\theta) = \exp(im\theta)$ (with $m \in \mathbb{Z}$) the transverse and the azimuthal field distributions, respectively. We suppose that $T(r, z)$ is the fundamental transverse mode since mode-leaking associated to bending losses is more important for higher-order modes [21,37]. In this approximation the electric field of the TE-component is almost completely along the direction \mathbf{u}_r (then $\mathbf{u}_{\text{TE}} \perp \mathbf{u}_r$) and the magnetic field of the TM component is almost completely polarized along the direction $\mathbf{u}_{\text{TM}} \approx \mathbf{u}_r$. This fact in concurrence with a Type 0 FWM configuration with a quasi-TE pump allows us to consider the dynamics of the TE modes only since they are decoupled from TM modes and to reduce the full problem to a scalar one. Then the spatial modes of the displacement field have the form $\mathbf{d}_{f,m}(\mathbf{r}) = R(r, z) Y_{f,m}(\theta) \mathbf{u}$ and $\mathbf{u} \approx \mathbf{u}_r$.

Since we are in the context of a scalar theory, the nonlinear polarization is also along the radial vector \mathbf{u}_r and its component takes the form

$$\hat{P}_{\text{nl}}(\mathbf{r}, t) = -\epsilon_0 \eta^{(3)} D^3(\mathbf{r}, t), \quad (\text{A8})$$

where $\eta^{(3)}$ is the inverse permittivity tensor and assuming a medium with null second-order susceptibility.

APPENDIX B: THE HAMILTONIAN

The two terms, $\hat{H}_{p,p}$ and $\hat{H}_{p,s}$, in the interaction Hamiltonian \hat{H}_{int} Eq. (9) in the main text are

$$\begin{aligned} \hat{H}_{p,p} = & \frac{g_0}{6} \sum_{k,l,m,n} \mathcal{A}_{k,l}^{m,n} (\delta_{[k+l-m-n]} \hat{p}_k \hat{p}_l \hat{p}_m^\dagger \hat{p}_n^\dagger + \delta_{[k-l+m-n]} \\ & \times \hat{p}_k \hat{p}_l^\dagger \hat{p}_m \hat{p}_n^\dagger + \delta_{[k-l-m+n]} \hat{p}_k \hat{p}_l^\dagger \hat{p}_m^\dagger \hat{p}_n) + \text{H.c.}, \quad (\text{B1}) \end{aligned}$$

$$\begin{aligned} \hat{H}_{p,s} = & g_0 \sum_{k,l,m,n} \mathcal{B}_{k,l}^{m,n} (\delta_{[k+l-m-n-1]} \hat{p}_k \hat{p}_l \hat{s}_m^\dagger \hat{s}_n^\dagger + \delta_{[k-l+m-n]} \\ & \times \hat{p}_k \hat{p}_l^\dagger \hat{s}_m \hat{s}_n^\dagger + \delta_{[k-l-m+n]} \hat{p}_k \hat{p}_l^\dagger \hat{s}_m^\dagger \hat{s}_n) + \text{H.c.}, \end{aligned} \quad (\text{B2})$$

where ‘‘H.c.’’ denotes ‘‘Hermitian conjugate.’’ In these expressions, $\delta_{[.]}$ is the usual Kronecker symbol (equal to 1 when $[.] = 0$ and to 0 otherwise), g_0 is the nonlinear coupling constant,

$$g_0 = \frac{3\hbar^2 \epsilon_0^2 \eta^{(3)} \Lambda}{8} \quad (\text{B3})$$

and

$$\Lambda = \int_0^{+\infty} \int_{-\infty}^{+\infty} dr dz r |R(r, z)|^4, \quad (\text{B4})$$

$$\mathcal{A}_{k,l}^{m,n} = \sqrt{\omega_{p,k} \omega_{p,l} \omega_{p,m} \omega_{p,n}} \approx \omega_0^2, \quad (\text{B5})$$

$$\mathcal{B}_{k,l}^{m,n} = \sqrt{\omega_{p,k} \omega_{p,l} \omega_{s,m} \omega_{s,n}} \approx \omega_0^2. \quad (\text{B6})$$

APPENDIX C: QUANTUM LANGEVIN EQUATIONS

After removing the explicit time dependence by moving to the reference frame of the injection and defining new fields such that

$$\hat{p}_m \rightarrow \hat{p}_m e^{-i\bar{\omega}_p m t}, \quad (\text{C1})$$

$$\hat{s}_m \rightarrow \hat{s}_m e^{-i\bar{\omega}_s m t}, \quad (\text{C2})$$

the Heisenberg equations for pump and signal fields reads as:

$$\begin{aligned} \frac{d\hat{p}_j}{dt} = & -i\Delta_{p,j} \hat{p}_j + \mathcal{E}_j - i\frac{g}{3} \sum_{m,n} [\hat{p}_{m+n-j}^\dagger \hat{p}_m \hat{p}_n + \hat{p}_{m+n-j+1}^\dagger \hat{s}_m \hat{s}_n \\ & + \hat{p}_{j-m+n} (\hat{p}_m \hat{p}_n^\dagger + \hat{p}_n^\dagger \hat{p}_m + \hat{s}_m \hat{s}_n^\dagger + \hat{s}_n^\dagger \hat{s}_m)], \end{aligned} \quad (\text{C3})$$

$$\begin{aligned} \frac{d\hat{s}_j}{dt} = & -i\Delta_{s,j} \hat{s}_j - ig \sum_{m,n} [\hat{p}_{j-m+n+1} \hat{p}_m \hat{s}_n^\dagger \\ & + (\hat{p}_{j+m-n} \hat{p}_m^\dagger + \hat{p}_{m+n-j}^\dagger \hat{p}_m) \hat{s}_n], \end{aligned} \quad (\text{C4})$$

with $g = (2g_0\omega_0^2)/(\hbar)$, $\Delta_{p,j} = \omega_{p,j} - \bar{\omega}_{p,j}$, and $\Delta_{s,j} = \omega_{s,j} - \bar{\omega}_{s,j}$. They are frequency-dependent detunings that, after using Eq. (2) in the main text, can be expressed as

$$\Delta_{p,j} \approx \Delta_0 + \Delta\Omega(2j) + \frac{\Omega_2}{2!}(2j)^2, \quad (\text{C5})$$

$$\Delta_{s,j} \approx \Delta_0 + \Delta\Omega(2j+1) + \frac{\Omega_2}{2!}(2j+1)^2, \quad (\text{C6})$$

where $\Delta_0 = \omega_0 - \bar{\omega}_p$ is the detuning between the central cavity resonance (of order $j = 0$) and the external injection centered at frequency ω_p , $\Delta\Omega = \Omega_1 - \Omega_p/2$ is the mismatch between the average FSR and the half of the spacing of the external frequency comb. Langevin equations also include the effect of propagation losses inside the microring, that couples the pump and signal modes with the input vacuum modes $\hat{q}_{in,m}$ and $\hat{r}_{in,m}$ via the coefficients $\kappa_{p,m}$ and $\kappa_{s,m}$, respectively. In a similar way, losses due to the microring coupling with the straight guide introduce $\hat{p}_{in,j}$ and $\hat{s}_{in,m}$ via the coefficients $\gamma_{p,m}$ and $\gamma_{s,m}$. The explicit expression of the quantum Langevin

equations can then be obtained by employing standard open quantum systems methods [28]. They read as

$$\begin{aligned} \frac{d\hat{p}_j}{dt} = & -(\gamma_{p,j} + \kappa_{p,j} + i\Delta_{p,j})\hat{p}_j + \mathcal{E}_j + \sqrt{2\gamma_{p,j}}\hat{p}_{in,j} \\ & + \sqrt{2\kappa_{p,j}}\hat{q}_{in,j} - i\frac{g}{3} \sum_{m,n} [\hat{p}_{m+n-j}^\dagger \hat{p}_m \hat{p}_n + \hat{p}_{m+n-j+1}^\dagger \hat{s}_m \hat{s}_n \\ & + \hat{p}_{j-m+n} (\hat{p}_m \hat{p}_n^\dagger + \hat{p}_n^\dagger \hat{p}_m + \hat{s}_m \hat{s}_n^\dagger + \hat{s}_n^\dagger \hat{s}_m)], \end{aligned} \quad (\text{C7})$$

$$\begin{aligned} \frac{d\hat{s}_j}{dt} = & -(\gamma_{s,j} + \kappa_{s,j} + i\Delta_{s,j})\hat{s}_j + \sqrt{2\gamma_{s,j}}\hat{s}_{in,j} + \sqrt{2\kappa_{s,j}}\hat{r}_{in,j} \\ & - ig \sum_{m,n} [\hat{p}_{j-m+n+1} \hat{p}_m \hat{s}_n^\dagger + (\hat{p}_{j+m-n} \hat{p}_m^\dagger \\ & + \hat{p}_{m+n-j}^\dagger \hat{p}_m) \hat{s}_n]. \end{aligned} \quad (\text{C8})$$

APPENDIX D: LINEARIZED QUANTUM LANGEVIN EQUATIONS

Quantum Langevin equations (C7) and (C8) are now linearized around the system stable steady-state solutions, $\langle \hat{p}_m \rangle$ and $\langle \hat{s}_m \rangle$. This work focuses on the below threshold regime where the steady-state solutions for the signal exhibit null mean values, therefore we set $\langle \hat{s}_m \rangle = 0, \forall m$. On the other hand, the $\langle \hat{p}_m \rangle$ are found as solutions of the system of nonlinear (cubic) algebraic equations obtained from the classical part of Eq. (C7). This operation leads to a set of linear quantum Langevin equations for the signal modes expressed in terms of the quadrature column vector $\hat{\mathbf{R}}(t) = (\hat{\mathbf{x}}(t)|\hat{\mathbf{y}}(t))^T$:

$$\begin{aligned} \frac{d\hat{\mathbf{R}}(t)}{dt} = & (-\Gamma' - \mathcal{K} + \mathcal{M})\hat{\mathbf{R}}(t) + \sqrt{2\Gamma'}\hat{\mathbf{R}}_{in}^{(\gamma)}(t) \\ & + \sqrt{2\mathcal{K}}\hat{\mathbf{R}}_{in}^{(\kappa)}(t), \end{aligned} \quad (\text{D1})$$

where the matrices $\Gamma' = \text{diag}\{\gamma|\gamma\}$ and $\mathcal{K} = \text{diag}\{\kappa|\kappa\}$ are diagonal matrices containing the mode-dependent cavity losses due to the microring coupling $\gamma = \text{diag}\{\dots, \gamma_{s,-1}, \gamma_{s,0}, \gamma_{s,1}, \dots\}$ and propagation losses $\kappa = \text{diag}\{\dots, \kappa_{s,-1}, \kappa_{s,0}, \kappa_{s,1}, \dots\}$. The input mode quadratures are collected in the column vectors $\hat{\mathbf{R}}_{in}^{(\gamma)}(t)$ and $\hat{\mathbf{R}}_{in}^{(\kappa)}(t)$ which are the quadratures of $(\dots, \hat{s}_{in,-1}, \hat{s}_{in,0}, \hat{s}_{in,+1}, \dots)^T$ and $(\dots, \hat{r}_{in,-1}, \hat{r}_{in,0}, \hat{r}_{in,+1}, \dots)^T$, respectively, and we suppose they are both in vacuum state. The intermodal coupling matrix \mathcal{M} can be expressed as

$$\mathcal{M} = \begin{pmatrix} \text{Im}[G+F] & \text{Re}[G-F] \\ -\text{Re}[G+F] & -\text{Im}[G+F]^T \end{pmatrix}, \quad (\text{D2})$$

where the matrices G and F are such that

$$F_{j,n} = g \sum_m \langle \hat{p}_{j-m+n+1} \rangle \langle \hat{p}_m \rangle, \quad (\text{D3})$$

$$G_{j,n} = \Delta_{s,j} \delta_{[j-n]} + g \sum_m 2 \langle \hat{p}_{j+m-n} \rangle \langle \hat{p}_m \rangle^*. \quad (\text{D4})$$

Hence $G = G^\dagger$ is an Hermitian complex matrix and $F = F^T$ is symmetric. These properties make \mathcal{M} an Hamiltonian matrix, that is $(\Omega\mathcal{M})^T = \Omega\mathcal{M}$, with Ω the symplectic form.

APPENDIX E: FROM DOUBLE-BUS TO SINGLE-BUS CAVITY LANGEVIN EQUATIONS

In order to apply the theory we developed in Ref. [18], we map Eq. (D1) to the linear quantum Langevin equation of a single-bus cavity. This is obtained by defining [29]

$$\hat{\mathbf{R}}_{\text{in}}(t) = \frac{\sqrt{2\Gamma'}\hat{\mathbf{R}}_{\text{in}}^{(\gamma)}(t) + \sqrt{2\mathcal{K}}\hat{\mathbf{R}}_{\text{in}}^{(\kappa)}(t)}{\sqrt{2(\Gamma' + \mathcal{K})}}. \quad (\text{E1})$$

Hence we get the quantum Langevin equation (2) considered in the main text

$$\frac{d\hat{\mathbf{R}}(t)}{dt} = (-\Gamma + \mathcal{M})\hat{\mathbf{R}}(t) + \sqrt{2\Gamma}\hat{\mathbf{R}}_{\text{in}}(t), \quad (\text{E2})$$

with $\Gamma = \Gamma' + \mathcal{K}$. Then, by using the input-output relation $\hat{\mathbf{R}}_{\text{out}}^{(\gamma)} = \sqrt{\Gamma'}\hat{\mathbf{R}} - \hat{\mathbf{R}}_{\text{in}}^{(\gamma)}$, the field quadratures at the output coupler $\hat{\mathbf{R}}_{\text{in}}^{(\gamma)}(t)$ are given by

$$\hat{\mathbf{R}}_{\text{out}}^{(\gamma)} = \sqrt{\frac{\Gamma'}{\Gamma}}\hat{\mathbf{R}}_{\text{out}} + \sqrt{\frac{\Gamma'\mathcal{K}}{\Gamma^2}}\hat{\mathbf{R}}_{\text{in}}^{(\kappa)} - \left(1 - \frac{\Gamma'}{\Gamma}\right)\hat{\mathbf{R}}_{\text{in}}^{(\gamma)}, \quad (\text{E3})$$

where the definition of $\hat{\mathbf{R}}_{\text{out}}$ is given by (E1) after replacing “in” by “out” everywhere. This column vector contains the quadratures of field operators at the output of a virtual system having only one source of losses (single-bus model).

APPENDIX F: HIGHER-ORDER MORPHING SUPERMODES

In the main text we illustrated only the first morphing supermodes. In this section we show the structure of the second, third, and fourth morphing supermodes for the different configurations discussed in the main text. Note that real and part imaginary part of $U_m(\omega)$ are respectively symmetric and antisymmetric with respect to the exchange of ω with $-\omega$ as expected due to the symmetry property $\hat{\mathbf{R}}_{\text{out}}^\dagger(\omega) = \hat{\mathbf{R}}_{\text{out}}(-\omega)$.

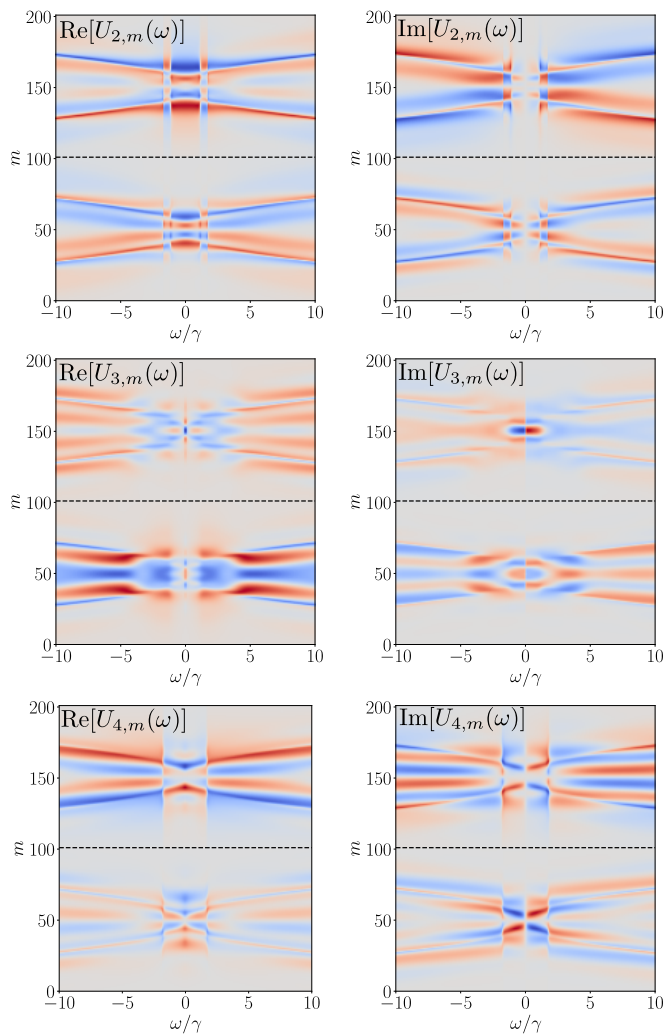


FIG. 7. Real and imaginary part of the second, third, and fourth morphing supermodes corresponding to the configuration of Fig. 4 in the main text.

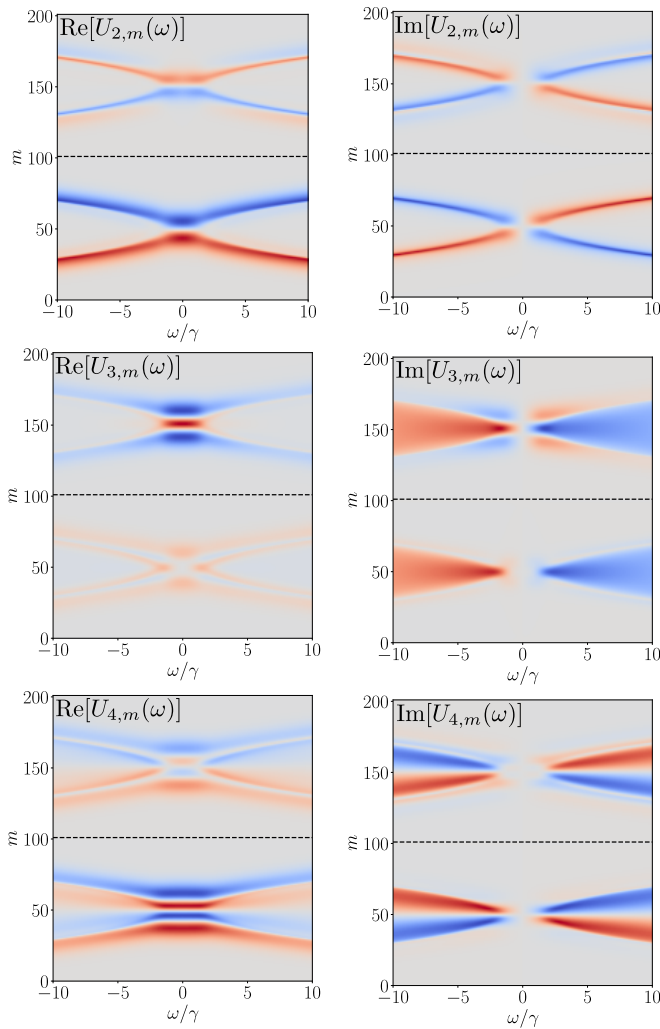


FIG. 8. Real and imaginary part of the second, third, and fourth morphing supermodes corresponding to the configuration of Fig. 5 (left) in the main text, with dispersion.

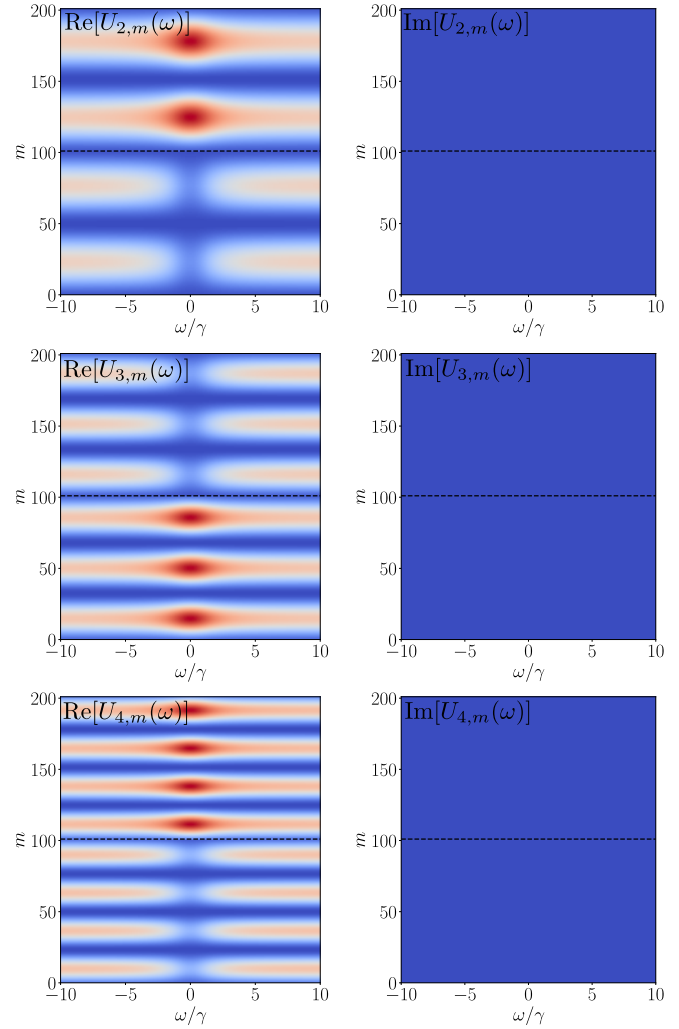


FIG. 9. Real and imaginary part of the second, third and fourth morphing supermodes corresponding to the configuration of Fig. 5 (right) in the main text, without dispersion.

[1] J. Wang, F. Sciarrino, A. Laing, and M. G. Thompson, Integrated photonic quantum technologies, *Nat. Photon.* **14**, 273 (2020).

[2] D. Oser, S. Tanzilli, F. Mazeas, C. Alonso-Ramos, X. Le Roux, G. Sauder, X. Hua, O. Alibart, L. Vivien, E. Cassan, and L. Labonté, High-quality photonic entanglement out of a stand-alone silicon chip, *npj Quant. Inf.* **6**, 31 (2020).

[3] P. Imany, J. A. Jaramillo-Villegas, O. D. Odele, K. Han, D. E. Leaird, J. M. Lukens, P. Lougovski, M. Qi, and A. M. Weiner, 50-GHz-spaced comb of high-dimensional frequency-bin entangled photons from an on-chip silicon nitride microresonator, *Opt. Express* **26**, 1825 (2018).

[4] H. Mahmudlu, R. Johanning, A. K. Kashi, A. van Rees, J. P. Epping, R. Haldar, K.-J. Boller, and M. Kues, Fully on-chip photonic turnkey quantum source for entangled qubit/qudit state generation, *Nat. Photon.* **17**, 518 (2023).

[5] M. Kues, C. Reimer, J. M. Lukens, W. J. Munro, A. M. Weiner, D. J. Moss, and R. Morandotti, Quantum optical microcombs, *Nat. Photon.* **13**, 170 (2019).

[6] A. Dutt, K. Luke, S. Manipatruni, A. L. Gaeta, P. Nussenzveig, and M. Lipson, On-chip optical squeezing, *Phys. Rev. Appl.* **3**, 044005 (2015).

[7] V. D. Vaidya, B. Morrison, L. G. Helt, R. Shahrokshahi, D. H. Mahler, M. J. Collins, K. Y. Tan, J. Lavoie, A. Repington, M. Menotti, N. Quesada, R. C. Pooser, A. E. Lita, T. Gerrits, S. W. Nam, and Z. Vernon, Broadband quadrature-squeezed vacuum and nonclassical photon number correlations from a nanophotonic device, *Sci. Adv.* **6**, eaba9186 (2020).

[8] Y. Zhao, Y. Okawachi, J. K. Jang, X. Ji, M. Lipson, and A. L. Gaeta, Near-Degenerate Quadrature-Squeezed Vacuum Generation on a Silicon-Nitride Chip, *Phys. Rev. Lett.* **124**, 193601 (2020).

[9] Z. Yang, M. Jahanbozorgi, D. Jeong, S. Sun, O. Pfister, H. Lee, and X. Yi, A squeezed quantum microcomb on a chip, *Nat. Commun.* **12**, 4781 (2021).

- [10] J. M. Arrazola, V. Bergholm, K. Brádler, T. R. Bromley, M. J. Collins, I. Dhand, A. Fumagalli, T. Gerrits, A. Goussev, L. G. Helt, J. Hundal, T. Isacson, R. B. Israel, J. Izaac, S. Jahangiri, R. Janik, N. Killoran, S. P. Kumar, J. Lavoie, A. E. Lita *et al.*, Quantum circuits with many photons on a programmable nanophotonic chip, *Nature (Lond.)* **591**, 54 (2021).
- [11] Y. K. Chembo, Quantum dynamics of kerr optical frequency combs below and above threshold: Spontaneous four-wave mixing, entanglement, and squeezed states of light, *Phys. Rev. A* **93**, 033820 (2016).
- [12] M. A. Guidry, D. M. Lukin, K. Y. Yang, R. Trivedi, and J. Vučković, Quantum optics of soliton microcombs, *Nat. Photon.* **16**, 52 (2022).
- [13] C. Fabre and N. Treps, Modes and states in quantum optics, *Rev. Mod. Phys.* **92**, 035005 (2020).
- [14] L. Dellantonio, A. S. Sørensen, and D. Bacco, High-dimensional measurement-device-independent quantum key distribution on two-dimensional subspaces, *Phys. Rev. A* **98**, 062301 (2018).
- [15] N. C. Menicucci, S. T. Flammia, H. Zaidi, and O. Pfister, Ultra-compact generation of continuous-variable cluster states, *Phys. Rev. A* **76**, 010302(R) (2007).
- [16] G. Patera, C. Navarrete-Benlloch, G. J. de Valcárcel, and C. Fabre, Quantum coherent control of highly multipartite continuous-variable entangled states by tailoring parametric interactions, *Eur. Phys. J. D* **66**, 241 (2012).
- [17] F. Arzani, C. Fabre, and N. Treps, Versatile engineering of multimode squeezed states by optimizing the pump spectral profile in spontaneous parametric down-conversion, *Phys. Rev. A* **97**, 033808 (2018).
- [18] E. Gouzien, S. Tanzilli, V. D'Auria, and G. Patera, Morphing Supermodes: A Full Characterization for Enabling Multimode Quantum Optics, *Phys. Rev. Lett.* **125**, 103601 (2020).
- [19] F. A. S. Barbosa, A. S. Coelho, K. N. Cassemiro, P. Nussenzveig, C. Fabre, M. Martinelli, and A. S. Villar, Beyond Spectral Homodyne Detection: Complete Quantum Measurement of Spectral Modes of Light, *Phys. Rev. Lett.* **111**, 200402 (2013).
- [20] F. A. S. Barbosa, A. S. Coelho, K. N. Cassemiro, P. Nussenzveig, C. Fabre, A. S. Villar, and M. Martinelli, Quantum state reconstruction of spectral field modes: Homodyne and resonator detection schemes, *Phys. Rev. A* **88**, 052113 (2013).
- [21] V. Van, *Optical Microring Resonators: Theory, Techniques, and Applications*, 1st ed. (CRC Press, Boca Raton, FL, 2016).
- [22] J. Roslund, R. M. de Araújo, S. Jiang, C. Fabre, and N. Treps, Wavelength-multiplexed quantum networks with ultrafast frequency combs, *Nat. Photon.* **8**, 109 (2014).
- [23] P. D. Drummond and M. Hillery, Quantum theory of dispersive electromagnetic modes, *Phys. Rev. A* **59**, 691 (1999).
- [24] N. Quesada and J. E. Sipe, Why you should not use the electric field to quantize in nonlinear optics, *Opt. Lett.* **42**, 3443 (2017).
- [25] M. G. Raymer, Quantum theory of light in a dispersive structured linear dielectric: A macroscopic hamiltonian tutorial treatment, *J. Mod. Opt.* **67**, 196 (2020).
- [26] G. J. de Valcárcel, G. Patera, N. Treps, and C. Fabre, Multimode squeezing of frequency combs, *Phys. Rev. A* **74**, 061801(R) (2006).
- [27] G. Patera, N. Treps, C. Fabre, and G. J. de Valcárcel, Quantum theory of synchronously pumped type i optical parametric oscillators: Characterization of the squeezed supermodes, *Eur. Phys. J. D* **56**, 123 (2010).
- [28] C. W. Gardiner and P. Zoller, *Quantum Noise*, 3rd ed., Springer Series in Synergetics (Springer, Berlin, 1991).
- [29] E. Gouzien, Optique quantique multimode pour le traitement de l'information quantique, Ph.D. thesis, Université Côte d'Azur, 2019.
- [30] We are using the following notation: $[\cdot]^T$ for the transpose, $[\cdot]^*$ for the complex conjugate and $[\cdot]^\dagger$ for the Hermitian transpose.
- [31] Any matrix-valued transformation $S(\omega)$ is ω symplectic (see Ref. [18]) if it is a smooth $2N \times 2N$ complex matrix-valued function of the parameter ω (in our case the analysis frequency) such that, for every value of that parameter, the corresponding matrix is conjugate symplectic, i.e., $S(\omega)\Omega S^\dagger(\omega) = \Omega$, being $\Omega = \begin{pmatrix} 0 & I \\ -I & 0 \end{pmatrix}$ the N -mode symplectic form and I the $N \times N$ identity matrix.
- [32] In time domain the quadrature operators are defined such that their commutator is $[\hat{R}_m(t)\hat{R}_n(t')] = i\Omega_{m,n}\delta(t-t')$, with $\Omega_{m,n}$ the elements of the symplectic form Ω (see Ref. [31]). In Fourier domain $[\hat{R}_m(\omega)\hat{R}_n(\omega')] = i\Omega_{m,n}\delta(\omega+\omega')$.
- [33] M. I. Kolobov and G. Patera, Spatiotemporal multipartite entanglement, *Phys. Rev. A* **83**, 050302(R) (2011).
- [34] V. D'Auria, S. Fornaro, A. Porzio, S. Solimeno, S. Olivares, and M. G. A. Paris, Full Characterization of Gaussian Bipartite Entangled States by a Single Homodyne Detector, *Phys. Rev. Lett.* **102**, 020502 (2009).
- [35] H. El Dirani, Development of high quality silicon nitride chips for integrated nonlinear photonics, Ph.D. thesis, Université de Lyon, 2019.
- [36] A. C. Turner, C. Manolatu, B. S. Schmidt, M. Lipson, M. A. Foster, J. E. Sharping, and A. L. Gaeta, Tailored anomalous group-velocity dispersion in silicon channel waveguides, *Opt. Expr.* **14**, 4357 (2006).
- [37] M.-K. Chin, C. Xu, and W. Huang, Theoretical approach to a polarization-insensitive single-mode microring resonator, *Opt. Expr.* **12**, 3245 (2004).